The Role of High Frequency Dynamic Threshold (HiDT) Serum Carcinoembryonic Antigen (CEA) Measurements in Colorectal Cancer Surveillance

Grossmann, Irene; Verberne, Charlotte; De Bock, Geertruida; Havenga, Klaas; Kema, Ido; Klaase, Joost; Renehan, Andrew; Wiggers, Theo

Published in:
Cancers

DOI:
10.3390/cancers3022302

Publication date:
2011

FORMATION OF NANOTUBULAR TiO_2 STRUCTURES WITH VARIED SURFACE CHARACTERISTICS FOR BIOMATERIAL APPLICATIONS

Robinson Aguirre [1]*, Mónica Echeverry-Rendón[1,2,3], David Quintero[1], Juan G. Castaño [1], Martin C. Harmsen[3], Sara Robledo[2] , Félix Echeverría E. [1]

[1]Centro de Investigación, Innovación y Desarrollo de Materiales (CIDEMAT), Facultad de Ingeniería, Universidad de Antioquia, Calle 70 No. 52-21, Medellín, Colombia

[2] Programa de Estudio y Control de Enfermedades Tropicales (PECET), Instituto de Investigaciones Médicas, Facultad de Medicina, Universidad de Antioquia, Calle 70 No. 52-21, Medellín, Colombia

[3] University of Groningen, University Medical Center Groningen, Department of Pathology and Medical Biology, Hanzeplein 1-EA11, NL-9713 GZ Groningen, The Netherlands

* Corresponding author at: robinson.aguirre@udea.edu.co Tel: (+574)2196617, Fax: (+57) 2191051

This article has been accepted for publication and undergone full peer review but has not been through the copyediting, typesetting, pagination and proofreading process which may lead to differences between this version and the Version of Record. Please cite this article as an 'Accepted Article', doi: 10.1002/jbm.a.36331

Abstract

Nanotubular structures were generated on the surface of titanium c.p. by anodization technique in an aqueous solution of acetic acid (14% v/v) with different sources of fluoride ion (HF, NaF, NH_4F). The aim of using these three different compounds is to study the effect of the counterion (H^+, Na^+ and NH_4^+) on the morphology, wettability and surface free energy of the modified surface. Nanotubes were generated at 10 and 15 V for each anodizing solution. To further improve surface characteristics, the samples were heat-treated at 600ºC for 4 hours and at 560ºC for 3 hours. SEM images revealed the formation of nanotubes in all anodizing conditions, while their diameter increased proportionally to the electric potential. X-ray diffraction and micro-Raman spectroscopy results showed the presence of both anatase and rutile phases, with a higher content of rutile in the coatings obtained using NH_4F and an applied potential of 10 V. The heat-treatment significantly increased the wettability of the anodic coatings, especially for the coating obtained at 15 V with HF, which showed values < 7 degrees of contact angle. Besides, the nanotubes show a decrease in diameter due to the heat treatment, except for the nanotubes formed in NH_4F. Depending on their surface properties (e.g.. low contact angle and high surface free energy), these coatings potentially have great potential in biomedical applications, sensors devices, and catalytic applications among others.

Keywords: Wettability, Anodizing, Osteoblasts, Adipose tissue-derived stromal cells, TiO_2 Nanotubes.

1. INTRODUCTION

Titanium is (clinically) widely used because of its properties such as low density, high mechanical strength, and high corrosion resistance [(1),(2)]. All these properties allow its application in implantology and orthopedic implants. This material shows a high corrosion resistance in human body fluids, which is due to the formation of a passive coating of titanium dioxide (TiO_2). This coating increases its chemical stability and delays the release of titanium ions [(3)(4)]. However, for specific clinical applications as implants [(5)–(7)], a more tunable surface coating is required. Among the different techniques of surface modification, anodization is as an attractive alternative, because of its easy implementation, versatility and low cost. Anodization is an electrochemical technique that allows the modification of the characteristics of the oxide film to obtain different nanotopographies. The formation of titanium dioxide nanotubes using the anodization process has been widely employed. This process allows an easy control of the nanotubes properties (for examples morphology and internal diameter) through anodizing variables such as applied potential, current and electrolyte composition [(8)]. Titanium modified with surface nanotubular structures has potential in clinical applications, due to its excellent biocompatibility. Some authors [(9)–(12)] reported an increase in the adhesion and proliferation of cells in presence of nanotubular structures, but the effect of the diameter in the biological behavior is under discussion, some authors report the benefits of an internal diameter less than 30 nm in the biological performance [(13)–(16)], on the other hand, some authors report an increase on the biological performance in nanotubular structures with an internal diameter greater than 100 nm[(17)–(20)]. The use of fluoride ions in the solute augments formation of

nanotubes[18]–[23]. Investigators used aqueous acetic acid based electrolytes such as HF solutions [22]–[26] or water free acetic acid based electrolytes with NH_4F [27], but, to the best of our knowledge, the use of NH_4F or NaF in aqueous acetic acid based electrolytes has not been studied yet. In the current research, anodization of titanium in an acetic acid solution has been employed to obtain nanotubes with a wide range of diameters. In this work, we studied the effect of different fluoride ion sources (HF, NaF and NH_4F) together with extensive heat treatment, on the porous morphology, wettability and surface free energy of the anodic coatings and consequently on the biological response, in terms of adhesion and proliferation of adipose tissue-derived stromal cells (ASC).

2. MATERIALS AND METHODS

2.1 Samples Anodization

Square samples of c.p titanium, grade 2 (ASTM F-67)[28], with an area of 2 cm^2 and 1 mm of thickness were mechanically polished with SiC paper up to grade 2000, mirror polished with alumina powder (1 μm) and finally cleaned in acetone for 20 minutes in an ultrasonic bath.

Subsequently, the samples were anodized at voltages of 10 and 15 V in 100 mL of aqueous solution with 14 vol% (2.5 M) in acetic acid and 1 wt% of the different sources of fluoride ion ((0.36 M) HF, (0.24 M) NaF and (0.27 M) NH_4F). The anodic coatings were obtained using a DC power supply (Kepco BHK 500-0.4 MG) and the current data was recorded during 1 hour of anodization. The electrochemical cell used in the anodizing process was composed by two electrodes, the titanium sample was set as anode and a platinum mesh was used

as cathode. When the anodizing process was terminated, the samples were extracted rapidly from the anodized solution and cleaned with deionized water and dried in a cold air stream.

2.2 Coatings characterization

The morphology of the coatings was observed by scanning electron microscopy (SEM) using a JEOL JSM 6940 LV instrument. The thickness measurements was made through scratching the surface and inclining the sample to take the SEM image. Two different heat treatments was carried out, for the 15 V coatings at 600 °C during 4 hours, and, due to the nanotube structure was lost due the 600 °C heat treatment in the 10 V coating, a heat treatment at 560 °C during 3 hours was carried out. The crystalline phases after heat treatment was determined by X-ray diffraction (XRD), using a PANanalytical EMPYREAM instrument with Cu Kα radiation and 2θ scan from 10 to 95 degrees. The equipment used for micro-Raman spectroscopy was a Micro-Raman Jovin Yvon Horiba, Model Labram High Resolution. The internal diameter was measured using the public domain software image J. For each condition analyzed, 20 measures were taken.

The conductivity was measured with autolab 302 potentiostat through electrochemical impedance spectroscopy in the open circuit potential (OCP) using a platinum plate as working electrode with an area of 0.99 cm^2 , the distance between working electrode and counter electrode was 1.2 cm , the frequency range was 100 MHz-1Hz and the amplitude signal was 1 mV.

The contact angle measurements were carried out using a Goniometer/Tensiometer Ramé-hart Model 250 Standard with water as test liquid.

The surface free energy (SFE) calculations was developed with the Neumann method, whose equation is:

$$\cos\theta = 2\left(\frac{\gamma_S}{\gamma_L}\right)^{0.5} \exp\left[-\beta\left(\gamma_L - \gamma_S\right)^2\right] - 1 \quad \textbf{(1)}$$

With β = 0.0001247 $(m^2/mJ)^2$, γ_L =72.8 mJ/m^2, θ the contact angle measured for each specimen and γ_S the surface free energy. For solve the Neumann equation numerical methods was required.

2.3 Cytotoxicity test

Human osteoblastic osteosarcoma cell line SAOS-2 (ATCC® HTB-85™) was used to assess cytotoxicity. With this purpose, osteoblasts at a concentration of 5,000 cells/cm^2 were seeded on the different modified samples (including samples without anodizing), which were previously sterilized by autoclaving. Cells cultured on standard tissue culture-treated polystyrene plates were used as control. Cells and materials were incubated at 37 °C for 96h. Then, the mitochondrial activity was measured by MTT assay in which (3-(4,5-dimethylthiazol-2-yl)-2,5-diphenyltetrazolium bromide) at a concentration of 5 mg/ml in PBS was added and incubated for 4 h. After that, medium was removed and formazan crystals were dissolved by addition of SDS (Sodium dodecyl sulfate). Finally, absorbance was measured in a microplate reader at 570 nm. All the formulations were evaluated in two independent experiments and in triplicate. All results from treatments were normalized to the control.

2.4 Cell-Material Interaction

Osteoblasts were seeded at a density of 10.000cell/cm^2 on samples of differently modified titanium surfaces. Cells were cultured for 48h. After that, cells were fixed with 2.5% glutaraldehyde (overnight) and dehydrated in graded ethanol series (50%, 70%, 80%, 90% and 100%). Samples were dried in a critical point dryer (Samdri-795), sputter coated with gold (Dentom Vacuum Desk IV) and analyzed using SEM (SEM, JEOL JSM-6490LV).

2.5 Cell adhesion

Adipose tissue-derived stromal cells (ASC) were used to evaluate cell attachment at different times on the anodized samples with heat treatment. For this purpose 10,000 cells/cm^2 were seeded. After 3h, 6h, 12h and 24h the samples were washed twice with PBS and fixed with 4% paraformaldehyde in PBS for 30 min. Cytoskeleton was stained with Phalloidin (Invitrogen, A12379) in a dilution of 1:250 and Dapi (Sigma, D9542). Images were acquired with an Axio Observer Z1 inverted microscope (Carl Zeiss Microscopy, Jena) equipped with TissueFAXS acquisition software version 2.0.4 (TissueGnostics)

3. RESULTS

3.1 Anodizing process

Fig 1. shows the current vs. time behavior for the anodic coatings obtained using the three different sources of fluoride ion with applied voltages of 10 and 15 V. The curves have the typical form observed in nanotubes formation processes [(29)–(31)]. In the initial stage, the current quickly rose and immediately decreased until a

minimum value as a consequence of the formation of an oxide compact layer. Subsequently, the current slightly increased again, due to nucleation of pores induced by fluoride ions in the anodizing bath. Finally, the current remained stable as a result of an equilibrium between formation and dissolution processes. Comparing the minimum current density values the following order can be stated NH_4F > NaF > HF; the same ordering can be obtained for the charge density values as shown in Table 1 for both of the two voltages evaluated.

3.2 Compositional analysis

XRD spectra of the samples after heat treatment are shown in Fig. 2. The peaks of titanium, rutile and anatase phases are observed. The mass fraction of rutile (f_r) was calculated using the Spurr and Myers' equation: $f_r = 1.26I_r/(I_a + 1.26I_r)$ [32]–[34] and the results are summarized in Table 3, where I_a and I_r are the intensities of strongest peaks of anatase and rutile showed in the XRD patterns; according to these results, in all cases the rutile phase is predominant, although effects on these ratios of both anodizing voltage and fluoride ion source is observed. As seen in Table 3, both the lower and higher f_r values are obtained in the NH_4F electrolyte.

Fig. 3 shows the micro Raman spectra for the samples before the heat treatment (Fig.3 (a)) and after the heat treatment (Fig.3 (b)). The Raman spectra for the coatings without heat treatment shows broad peaks around 150,450 and 600 cm^{-1} , the form of this spectra has been reported by others authors in previous works [35]–[37], and shows the amorphous nature of the nanotubes as anodized, those peaks can be assigned to the Ti-O bond vibrations. The presence of rutile and anatase

phase was corroborated in the heat treated samples (Fig.3 (b)). The vibrations near to 144,195,396,517 and 635 cm^{-1} can be attributed to the anatase phase, on the other hand, the vibrations around to 239,445, and 612 cm^{-1} can be assigned to the rutile phase. The weak peak and the weak shoulder near to 195 and 635 cm^{-1} respectively are only present in the coatings obtained at 15 V, besides, a very broad peaks near to 351 cm^{-1} is present in the spectra after the heat treatment, and this vibration is attributed to the O-O bond [38].The linear relationship in weight between the rutile and anatase was calculated for the Raman spectra with the equation reported by Hardcastle [38] and developed by Zhang et al [39]: $W_R/W_A = 3.64 \times (I_{445}/I_{396})$, and the results are summarized in Table 4, where I_{445} and I_{396} are the peaks intensities in 445 and 396 cm^{-1} .

3.3 Morphologic characterization

Figs. 4, 5, 6 and 7 show SEM micrographs for the porous anodic films obtained in acetic acid solutions containing three different fluoride ion sources, with and without heat treatment. The measurements of thickness and internal diameter are listed in Table 5. Fig.4 and Fig. 6 show that the coatings produced at both 10 and 15 V have a nanotubular structure, due to the presence of individual tubes; the nanotubes produced in all cases are irregular and resembling a polygonal shape. Fig. 5 and Fig 7 evidence that the coatings at 15 V and 10 V respectively after the heat treatment keep the nanotubular structure but the walls are wider compared with the coatings without heat treatment, thus the internal diameter was reduced (see Table 5). As a heat treatment consequence, the nanotubes thickness were

reduced in all evaluated coatings, the thickness measurements before and after the heat treatment are shown in Table 5.

3.4 Wettability and surface free energy (SFE)

The contact angle measurements and the SFE calculations are shown in Tables 6 and 7, respectively. The coatings obtained at 15 V with heat treatment displayed the lowest values of contact angle; on the contrary, the films obtained at 10 V for HF and NaF without heat treatment showed the highest values of contact angle. The anodic films produced at 10 V without heat treatment had a higher contact angle compared to the coatings obtained at 15 V without heat treatment. The SFE calculations are given in Table 7. The higher values of SFE were given at 15 V after the heat treatment, especially for the coatings produced in HF, but the coatings obtained in NaF and NH_4F also shown significant increases in the SFE, in contrast with the coatings produced at 10 V with HF and NaF, which had the lowest values of SFE.

3.5 Biological Behavior

Although the samples were treated with different solutions during anodizing, this did not affect the biocompatibility of the samples. Results of the measurement of the mitochondrial activity of the cells cultivated on the surfaces are shown in Table 8.

All surface coatings of titanium were non-cytotoxic irrespective of the applied voltage or electrolyte that was used. After seeding and culturing for 3, 6, 12 or 24h,

the interactions between sentinel cells and the differently coated materials was evaluated by microphotography by SEM (Fig. 8 and 9) or fluorescence microscopy after staining of (Fig. 10). Both techniques show that the cells had adhered to all the surfaces.

Seeded osteoblasts showed a fast adherence already after 3h (Fig. 10), irrespective of the type of solute that was used to generate the anodized coating. Over the course of 24h, the number of adhering osteoblasts increased until the entire surface was virtually covered with the exception of bare titanium. The morphology of the cells changed from rounded (in particular on bare titanium) to stretched after some time after seeding. This indicates that the osteoblasts prefer surface-modified titanium for adhesion and stretching.

Discussion

One possible explanation of the current behavior is based on the electrolyte chemistry, since both NaF and NH_4F totally dissociate in aqueous solution whilst HF is a weak acid with a dissociation constant (Ka) of 6.8 $x10^{-4}$, and in acidic solution (i.e. acetic acid), thus, principally exists in HF form [9]. As a result, a lower quantity of fluoride ions is present in electrolytes with HF in comparison with NaF and NH_4F, thus the conductivity in the NaF and NH_4F based electrolytes is bigger than in the HF based electrolytes (see Table 2). Therefore, the minimum value of current density is directly related with the conductivity, The bigger the conductivity, the higher the minimum value of current; this behavior has been reported in literature by Lee et al [40] , Zhang et al [41] and Lee et al[42].

For the HF solute the ratio (f_r) is similar for both anodizing voltages, whereas for the NaF and NH_4F baths an opposite effect of the applied voltage is obtained, in the former the mass fraction of rutile increases with voltage and for the latter it decreases.

The thickness increase with the applied potential rise in all coatings obtained, as reported in previous works [43]–[45]. In the same way, the thickness increase with the conductivity rise. K. Lee et al reported [42] a linear relationship between conductivity and thickness. In all cases, as the voltage is risen also the internal nanotube diameter increases, the direct relationship between internal diameter and applied potential has been described in previous studies [29],[31],[46]. According with Regonini et al [29] the applied potential is responsible for the electric field strength along the oxide coating, affecting principally the ion migration and thus the nanotube internal diameter. The internal nanotube diameter of samples formed at 10 V is similar (around 30 nm) with a slightly bigger diameter for the sample treated in a NaF containing solution. When the anodizing voltage is risen to 15 V the diameter obtained is very similar for HF and NaF samples (approx. 67 nm) whilst for the NH_4F sample is much lower (approx. 49 nm). One possible explanation about the differences in the internal diameter of the nanotubes can be based in the electrolyte conductivity; according with the data in Table 2, the electrolyte conductivity decreases in this order: NH4F > NaF> HF. Y.Zhang et al[41] and K. Lee et al [42] found different morphologies in nanotubes formed at different values of conductivity and Sopha et al [44] reported an increase in internal diameter proportional to the increment of the conductivity for nanotubes produced in organic media. However, in this research work it was found that despite big differences in electrolyte conductivities it does not show a relationship with the internal diameter

of the nanotubes formed; for example, for the electrolyte with higher conductivity (NH_4F), the lower nanotube internal diameter is obtained at 15 V of anodizing voltage, whereas electrolytes with different values of conductivity (NaF and HF), produced similar values of internal diameter. Some authors like Wen Xin et al [23] Zhao et al [25] report similar values of internal diameter using aqueous acetic acid based electrolytes with HF.

For all coatings analyzed after the heat treatment, the rutile phase is present in high proportion compared with the anatase phase, which corroborate the results of the XRD spectra. In the HF and NaF baths, the ratio is directly proportional to the applied potential, in contrast with the NH_4F bath, the ratio (W_R/W_A) is inversely proportional to the applied potential. The lower value is obtained in the NH_4F bath, while, the highest value is obtained in the HF bath.

This internal diameter reduction (see Table 5) as a consequence of the heat treatment has been previously reported from other authors [47]–[49] as a consequence of the transformation from amorphous to rutile phase. According with Zhang et al [49], there are three nucleation forms of rutile phase with a strong dependence of temperature and heat treatment time: surface, interface and bulk nucleation. Heat treatments at low temperatures (<650^{o}C), interface nucleation and surface nucleation are predominant. On the other hand, bulk nucleation is the principal nucleation form at high temperatures (>650^{o}C). Time is another important factor in the nucleation process for ensuring phase transformation, but an exaggerated time is critical for the stability of the coating. For the temperature and time used (600°C and 4 hours , and 560°C and 3 hours) in the present study, surface nucleation is expected to be the predominant process. Consequently, the

internal diameter was reduced for the increment of the wall thickness. Yu et al [48] reported similar results in the morphology of TiO_2 nanotubes after the heat treatment at 700°C. Fig. 5(e) shows a crack in the coating after the heat treatment as a result of a difference in the thermal coefficient between the titanium substrate and the TiO_2 coating, this phenomenon has been reported previously by Fang et al [50] after the heat treatment at 600°C. For the samples analyzed after the heat treatment, it is realized in this work, few cracks were observed. Besides the above, the thickness had a reduction as a heat treatment consequence, this phenomenon has been reported by several authors[50]–[53]. Shivaram et al[51] propose an explanation for this phenomenon based on the phase on thermal degradation. According with Shivaram the thickness reduction depends on the initial thickness, hold time and the temperature. This is in agreement with our results, due to, although, for the anodic coatings obtained at 15V the heat treatment has the same hold time and temperature, the thickness reduction was different, due to the differences in the coatings thickness before the heat treatment.

While comparing the data for the three fluoride ion sources, it is found that in addition to the nanotube diameter there are other factors strongly influencing the surface wettability of the samples, for instance, the chemistry of anodizing bath and the structural composition of the anodic oxide film. The decrease of the contact angle as a consequence of the heat treatment is evidenced in Table 6. Previous studies reported similar results [54][55], and the explanation resides in the characteristic of the rutile phase, which have a higher value of surface free energy (γ_{rutile}:~2.2 J m^{-2}, $\gamma_{anatase}$:~0.4 J m^{-2}, $\gamma_{amorphous}$:~0.35 J m^{-2}) [56][57] compared with the amorphous phase present before the heat treatment (see Fig. 3), and high SFE values are directly related with hydrophilicity [58] [59].

Analysis of the Table 7 data in conjunction with that of Table 3 does not indicates the existence of a clear relationship of SFE with the content of rutile in the oxide surface, therefore it appears that the SFE of a TiO_2 surface it not solely determined by its rutile content; surface chemistry and morphology might play an important role as indicated by the variation of SFE values obtained for either samples prepared in different anodizing baths or at different cell voltages. SFE is directly related with the capability of a surface to interact with the environment; a surface with a high surface energy is able to interact more easily with external agents, such as water and biological specimens. Nakamura et al [60] studied the effect of SFE on cell adhesion and they concluded that an increase in SFE accelerated this adhesion.

In regards with the counterion (H^+, Na^+ and NH_4^+) effect on the morphology, wettability and surface free energy of the anodized surfaces according with our results we can establish. First, the three kind of the anodized surfaces have the same nanotube morphology (irregular and resembling a polygonal shape), thus, the use of fluoride salts (Na^+ and NH_4^+) instead of hydrofluoric acid (H^+) does not increase the nanotube uniformity and organization. Besides the above, the thickness increases with the potential rise, also, the thickness is dependent of the conductivity value and in turn, the conductivity is influenced by the counterion. The higher the conductivity, the bigger the thickness. Second, before heat treatment, the anodic coatings obtained using NH_4F had the lowest contact angle for the two voltages evaluated. On the other hand the anodic coatings obtained using HF had the highest contact angle. After heat treatment, all evaluated surfaces had a hydrophilic behavior (CA<22°), but, the coating obtained using HF at 15V had the lowest contact angle.

The anodizing process does not affect the general biocompatibility of the samples, even though they were exposed to strong solutions. Heat treatment of metal surfaces increases their surface energy[61] as was also shown for the titanium surfaces (see Table 7). We surmised that fluoride anodized titanium surfaces would favor cell adhesion and might augment proliferation too. Thus high energy surfaces and non-heated controls, were assessed for these parameters using osteoblasts and adipose tissue-derived stromal cells (ASCs). Furthermore, these cells had formed filopodia-like protrusions that followed the topography of the coating (Fig. 8d, arrow heads). These cytoplasmic protrusions are observed in cells growing in the all the treated samples but in less proportion in cells on untreated surfaces. Filopodia are structures consist of microtubules and actin filaments and are used by cells to 'probe' the chemistry and biomechanics of their environment i.e. sense surfaces. Cells can respond to different patterns and scales of topography. Cells are moving over surfaces by recognizing different points of the structure and once a specific position is defined, lamellipodium structures are formed conducting the rest of the cell at that position. At this point, the cell experience a reconfiguration of the cytoskeleton where G-proteins signaling are involved [62]. According with Dalby, in materials that harbor a low cell adhesion, the number of filopodia is reduced due to the lack of adequate adhesive sites [62]. This relates to the surfaces characteristics. Attachment of cells are important in order to guide the synthesis and deposition of extracellular matrix and subsequently for the case of osteoblast to produce mineralization [63]. Results obtained in this work show a proper adhesion and behavior of cells on the modified surfaces with nanopatterns, further studies will investigate the influence of nanotopography osteogenic differentiation and the influence on therapeutic cells such as ASCs.

Previous studies support the fact that cells fates can be addressing for parameters in the environment such as topography, chemical composition, and surface energy among others [64]–[68]. In reference to the biological behavior, it is important to highlight that according to our results does not exist a specific experimental condition which is better than the others, at least, regarding toxicity of the material and cell-material interaction. At this point, we are able to confirm from the biological perspective that, first, the compounds used in the anodization process are not toxic, and second, that all the surfaces can promote cell adhesion.

4. CONCLUSIONS

TiO_2 nanotubes were successfully generated on titanium surfaces through anodization in acetic acid at potentials of 10 and 15 V and using different fluoride ion sources (HF, NaF, and NH_4F); the internal diameter of the nanotubes increased with the applied potential. After heat treatment, the coatings produced at 15 V keep the nanotubular structure while their internal diameter was reduced. In contrast, the coatings obtained at 10 V lost their nanotubular structure, and instead formed particulate aggregates. Due to heat treatment, the TiO_2 amorphous phase initially formed was replaced by anatase and rutile phases, with rutile as the predominant phase. The contact angle decreased after the heat treatment, being this decreasing higher at 15 V than at 10 V. After the heat treatment, SFE increases for all the coatings analyzed, this means in practical terms an increase in the surface properties. The bigger values of SFE were given at 15 V after the heat treatment, especially for the coatings produced in HF, but the coatings obtained in NaF and NH_4F also shown significant increases in the SFE, in contrast with the coatings

produced at 10 V with HF and NaF, which had the lowest values of SFE. From the biological side, paradigm about nano or micro patterning in surfaces are still in debate. However, results from this work show that nanotubes not affect the biocompatibility of the material and a proper attachment of cells on the coatings was observed. Since the coatings produced at 15 V after heat treatment showed interesting results due to their low contact angle and high SFE, biological assays did not show any conclusive difference with the other treatments. Nanotubes may be a proper reservoir of growth factors or drugs.

5. ACKNOWLEDGEMENTS

The authors are pleased to acknowledge the financial assistance of the "Departamento Administrativo de Ciencia, Tecnología e Innovación – COLCIENCIAS" through the project 111556933337 and "Estrategia de Sostenibilidad de la Universidad de Antioquia". M.E.R and R.A. are supported by COLCIENCIAS PhD grants.

6. REFERENCES

1. Kulkarni M, Patil-Sen Y, Junkar I, Kulkarni C V., Lorenzetti M, Iglič A. Wettability studies of topologically distinct titanium surfaces. Colloids and Surfaces B: Biointerfaces. 2015;129:47–53.

2. Tan a. W, Pingguan-Murphy B, Ahmad R, Akbar S a. Review of titania nanotubes: Fabrication and cellular response. Ceramics International. 2012;38:4421–35.

3. Quintero D, Galvis O, Calderón J a., Castaño JG, Echeverría F. Effect of electrochemical parameters on the formation of anodic films on commercially pure titanium by plasma electrolytic oxidation. Surface and Coatings Technology. 2014;258:1223–31.

4. Galvis OA, Quintero D, Castaño JG, Liu H, Thompson GE, Skeldon P, Echeverría F. Formation of grooved and porous coatings on titanium by plasma electrolytic oxidation in H2SO4/H3PO4 electrolytes and effects of coating morphology on adhesive bonding. Surface and Coatings Technology. 2015;269:238–49.

5. Wang N, Li H, Lü W, Li J, Wang J, Zhang Z, Liu Y. Effects of TiO2 nanotubes with different diameters on gene expression and osseointegration of implants in minipigs. Biomaterials. Elsevier Ltd; 2011;32:6900–11.

6. Von Wilmowsky C, Bauer S, Roedl S, Neukam FW, Schmuki P, Schlegel KA. The diameter of anodic TiO 2 nanotubes affects bone formation and correlates with the bone morphogenetic protein-2 expression in vivo. Clinical Oral Implants Research. 2012;23:359–66.

7. Von Wilmowsky C, Bauer S, Lutz R, Meisel M, Neukam FW, Toyoshima T, Schmuki P, Nkenke E, Schlegel KA. In Vivo Evaluation of Anodic TiO2 Nanotubes; An Experimental Study in the Pig. Journal of Biomedical Materials Research - Part B Applied Biomaterials. 2009;89:165–71.

8. Minagar S, Berndt CC, Wang J, Ivanova E, Wen C. A review of the application of anodization for the fabrication of nanotubes on metal implant surfaces. Acta biomaterialia. Acta Materialia Inc.; 2012;8:2875–88.

9. Das K, Bose S, Bandyopadhyay A. TiO2 nanotubes on Ti: Influence of nanoscale morphology on bone cell-materials interaction. Journal of biomedical materials research Part A. 2009;90:225–37.

10. Divya Rani V V., Vinoth-Kumar L, Anitha VC, Manzoor K, Deepthy M, Shantikumar VN. Osteointegration of titanium implant is sensitive to specific nanostructure morphology. Acta Biomaterialia. Acta Materialia Inc.; 2012;8:1976–89.

11. Oh S, Jin S. Titanium oxide nanotubes with controlled morphology for enhanced bone growth. Materials Science and Engineering: C. 2006;26:1301–6.

12. Hao YQ, Li SJ, Hao YL, Zhao YK, Ai HJ. Effect of nanotube diameters on bioactivity of a multifunctional titanium alloy. Applied Surface Science. 2013;268:44–51.

13. Park J, Bauer S, Von Der Mark K, Schmuki P. Nanosize and vitality: TiO2 nanotube diameter directs cell fate. Nano Letters. 2007;7:1686–91.

14. Park J, Bauer S, Schlegel KA, Neukam FW, von der Mark K, Schmuki P. TiO2 nanotube surfaces: 15 nm--an optimal length scale of surface topography for cell adhesion and differentiation. Small (Weinheim an der Bergstrasse, Germany). 2009;5:666–71.

15. Y.Q. Haoa, S.J. Lib, Y.L. Haob, Y.K. Zhaoc HJA. Effect of nanotube diameters on bioactivity of a multifunctional titanium alloy. Applied Surface Science. 2013;268:65–71.

16. Gongadze E, Kabaso D, Bauer S, Park J, Schmuki P, Iglič A. Adhesion of

osteoblasts to a vertically aligned TiO2 nanotube surface. Mini reviews in medicinal chemistry. 2013;13:194–200.

17. Yu W, Qian C, Jiang X, Zhang F, Weng W. Mechanisms of stem cell osteogenic differentiation on TiO2 nanotubes. Colloids and Surfaces B: Biointerfaces. Elsevier B.V.; 2015;136:779–85.

18. Zhang H, Yang S, Masako N, Lee DJ, Cooper LF, Ko C-C. Proliferation of preosteoblasts on TiO_2 nanotubes is FAK/RhoA related. RSC Adv. Royal Society of Chemistry; 2015;5:38117–24.

19. Roguska A, Pisarek M, Belcarz A, Marcon L, Holdynski M, Andrzejczuk M, Janik-Czachor M. Improvement of the bio-functional properties of TiO2 nanotubes. Applied Surface Science. 2016;388:775–85.

20. Zhang R, Wu H, Ni J, Zhao C, Chen Y, Zheng C, Zhang X. Guided proliferation and bone-forming functionality on highly ordered large diameter TiO2 nanotube arrays. Materials Science and Engineering C. Elsevier B.V.; 2015;53:272–9.

21. Bauer S, Park J, Pittrof A, Song Y-Y, Mark K, Schmuki P. Covalent functionalization of TiO2 nanotube arrays with EGF and BMP-2 for modified behavior towards mesenchymal stem cells. Integrative biology : quantitative biosciences from nano to macro. Aug 10, 2011. 927-936 p.

22. Mor GK, Varghese OK, Paulose M, Grimes C a. Transparent Highly Ordered TiO2 Nanotube Arrays via Anodization of Titanium Thin Films. Advanced Functional Materials. 2005;15:1291–6.

23. Xin W, Meng C, Jie W, Junchao T, Yan S, Ning D. Morphology dependence

of TiO 2 nanotube arrays on anodization variables and buffer medium. Journal of Semiconductors. 2010;31:63003.

24. Varghese OK, Mor GK, Paulose M, Grimes CA. A Titania Nanotube-Array Room-Temperature Sensor for Selective Detection of Low Hydrogen Concentrations. MRS Proceedings. 2004;828:A3.1-K4.1.

25. Zhao G, Lei Y, Zhang Y, Li H, Liu M. Growth and favorable bioelectrocatalysis of multishaped nanocrystal Au in vertically aligned TiO2 nanotubes for hemoprotein. Journal of Physical Chemistry C. 2008;112:14786–95.

26. Brammer KS, Oh S, Cobb CJ, Bjursten LM, van der Heyde H, Jin S. Improved bone-forming functionality on diameter-controlled TiO(2) nanotube surface. Acta biomaterialia. 2009;5:3215–23.

27. Tsuchiya H, Macak JM, Taveira L, Balaur E, Ghicov A, Sirotna K, Schmuki P. Self-organized TiO2 nanotubes prepared in ammonium fluoride containing acetic acid electrolytes. Electrochemistry Communications. 2005;7:576–80.

28. Standard Specification for Unalloyed Titanium, for Surgical Implant Applications (UNS R50250, UNS R50400, UNS R50550, UNS R50700). ASTM International; 2013.

29. Regonini D. a review of growt mechanism,structure and cristallinity of anodized TiO2 nanotubes. Materials Science and Engineering R. 2013;377–406.

30. Mor GK, Varghese OK, Paulose M, Shankar K, Grimes C a. A review on highly ordered, vertically oriented TiO2 nanotube arrays: Fabrication,

material properties, and solar energy applications. Solar Energy Materials and Solar Cells. 2006;90:2011–75.

31. Macak JM, Tsuchiya H, Ghicov a., Yasuda K, Hahn R, Bauer S, Schmuki P. TiO2 nanotubes: Self-organized electrochemical formation, properties and applications. Current Opinion in Solid State and Materials Science. 2007;11:3–18.

32. Sakurai K, Mizusawa M. X-ray Diffraction Imaging of Anatase and Rutile. Anal Chem. 2010;82:3519–22.

33. Liang H-C, Li X-Z. Effects of structure of anodic TiO(2) nanotube arrays on photocatalytic activity for the degradation of 2,3-dichlorophenol in aqueous solution. Journal of hazardous materials. 2009;162:1415–22.

34. Wu M, Long J, Huang A, Luo Y, Feng S, Xu R. Microemulsion-Mediated Hydrothermal Synthesis and Characterization of Nanosize Rutile and Anatase Particles. Langmuir. American Chemical Society; 1999;15:8822–5.

35. Zhao J, Wang X, Chen R, Li L. Fabrication of titanium oxide nanotube arrays by anodic oxidation. Solid State Communications. 2005;134:705–10.

36. Wang J, Lin Z. Freestanding TiO2 nanotube arrays with ultrahigh aspect ratio via electrochemical anodization. Chemistry of Materials. 2008;1257–61.

37. Podporska-Carroll J, Panaitescu E, Quilty B, Wang L, Menon L, Pillai SC. Antimicrobial properties of highly efficient photocatalytic TiO2 nanotubes. Applied Catalysis B: Environmental. Elsevier B.V.; 2015;176–177:70–5.

38. Hardcastle F. Raman Spectroscopy of Titania (TiO2) Nanotubular Water-Splitting Catalysts. Journal of the Arkansas Academy of Science.

2011;65:43–8.

39. Zhang J, Li M, Feng Z, Chen J, Li C. UV Raman Spectroscopic Study on TiO_2. I. Phase Transformation at the Surface and in the Bulk. J Phys Chem B. 2006;110:927–35.

40. Lee B-G, Choi J-W, Lee S-E, Jeong Y-S, Oh H-J, Chi C-S. Formation behavior of anodic TiO2 nanotubes in fluoride containing electrolytes. Transactions of Nonferrous Metals Society of China. 2009;19:842–5.

41. Zhang Y, Fan H, Ding X, Yan Q, Wang L, Ma W. Electrochimica Acta Simulation of anodizing current-time curves and morphology evolution of TiO 2 nanotubes anodized in electrolytes with different NH 4 F concentrations. Electrochimica Acta. Elsevier Ltd; 2015;176:1083–91.

42. Lee K, Kim H, Lee Y, Tak Y. Effect of Electrolyte Conductivity on the Formation of a Nanotubular TiO 2 Photoanode for a Dye-Sensitized Solar Cell. Journal of the Korean Physical Society. 2009;54:1027–31.

43. Sun L, Zhang S, Sun XW, He X. Effect of electric field strength on the length of anodized titania nanotube arrays. Journal of Electroanalytical Chemistry. Elsevier B.V.; 2009;637:6–12.

44. Sopha H, Hromadko L, Nechvilova K, Macak JM. Effect of electrolyte age and potential changes on the morphology of TiO2 nanotubes. Journal of Electroanalytical Chemistry. Elsevier B.V.; 2015;759:122–8.

45. Macak JM, Hildebrand H, Marten-Jahns U, Schmuki P. Mechanistic aspects and growth of large diameter self-organized TiO2 nanotubes. Journal of Electroanalytical Chemistry. 2008;621:254–66.

46. Roy P, Berger S, Schmuki P. TiO2 nanotubes: synthesis and applications. Angewandte Chemie (International ed in English). 2011;50:2904–39.

47. Jaroenworaluck a., Regonini D, Bowen CR, Stevens R. A microscopy study of the effect of heat treatment on the structure and properties of anodised TiO2 nanotubes. Applied Surface Science. 2010;256:2672–9.

48. Yu J, Wang B. Effect of calcination temperature on morphology and photoelectrochemical properties of anodized titanium dioxide nanotube arrays. Applied Catalysis B: Environmental. 2010;94:295–302.

49. Zhang H, Banfield JF. Phase Transformation of Nanocrystalline Anatase-to-Rutile Via Combined Interface and Surface Nucleation. Journal of Materials Research. 2000;15:437–48.

50. Fang D, Luo Z, Huang K, Lagoudas DC. Effect of heat treatment on morphology, crystalline structure and photocatalysis properties of TiO2 nanotubes on Ti substrate and freestanding membrane. Applied Surface Science. Elsevier B.V.; 2011;257:6451–61.

51. Shivaram A, Bose S, Bandyopadhyay A. Thermal degradation of TiO2 nanotubes on titanium. Applied Surface Science. 2014;317:573–80.

52. Lim YC, Zainal Z, Hussein MZ, Tan WT. The effect of heat treatment on phase transformation, morphology and photoelectrochemical response of short TiO2 nanotubes. Digest Journal of Nanomaterials and Biostructures. 2012;8:167–76.

53. Yang Y, Wang X, Li L. Crystallization and phase transition of titanium oxide nanotube arrays. Journal of the American Ceramic Society. 2008;91:632–5.

54. Zhao J, Wang X, Sun T, Li L. Crystal phase transition and properties of titanium oxide nanotube arrays prepared by anodization. Journal of Alloys and Compounds. 2007;434–435:792–5.

55. Yang L, Zhang M, Shi S, Lv J, Song X, He G, Sun Z. Effect of annealing temperature on wettability of TiO2 nanotube array films. Nanoscale research letters. 2014;9:621.

56. Navrotsky A. Energetics of nanoparticle oxides: interplay between surface energy and polymorphism. Geochemical transactions. 2003;4:34.

57. Stella K, Kovacs D a., Diesing D, Brezna W, Smoliner J. Charge Transport Through Thin Amorphous Titanium and Tantalum Oxide Layers. Journal of The Electrochemical Society. 2011;158:P65.

58. Hanaor D a H, Sorrell CC. Review of the anatase to rutile phase transformation. Journal of Materials Science. 2011;46:855–74.

59. Wang S, Liu Y, Zhang C, Liao Z, Liu W. The improvement of wettability, biotribological behavior and corrosion resistance of titanium alloy pretreated by thermal oxidation. Tribology International. Elsevier; 2014;79:174–82.

60. Nakamura M, Hori N, Ando H, Namba S, Toyama T, Nishimiya N, Yamashita K. Surface free energy predominates in cell adhesion to hydroxyapatite through wettability. Materials Science and Engineering: C. Elsevier B.V.; 2016;62:283–92.

61. Packham DE. Surface energy, surface topography and adhesion. International Journal of Adhesion and Adhesives. 2003;23:437–48.

62. Dalby MJ. Cellular response to low adhesion nanotopographies. International

journal of nanomedicine. Dove Press; 2007;2:373.

63. Radke P. Outcome after treatment of coronary in-stent restenosis Results from a systematic review using meta-analysis techniques. European Heart Journal. 2003;24:266–73.

64. Lee J, Kim C, Ph D, Lim Y, Kim M. Surface analyses of titanium substrate modified by anodization and nanoescale Ca-P deposition. 2007;45:795–804.

65. Allain JP, Echeverry-rendón M, Pavón JJ, Arias SL. Nanostructured Biointerfaces. Nanopatterning and Nanoscale Devices for Biological Applications. 2015.

66. Kulkarni M, Patil-Sen Y, Junkar I, Kulkarni C V., Lorenzetti M, Iglič A. Wettability studies of topologically distinct titanium surfaces. Colloids and Surfaces B: Biointerfaces. 2015;129:47–53.

67. Thevenot P, Hu W, Tang L. Surface Chemistry Influence Implant Biocompatibility. Current Topics in Medicinal Chemistry. 2008;8:270–80.

68. Deligianni DD, Katsala N, Ladas S, Sotiropoulou D, Amedee J, Missirlis YF. Effect of surface roughness of the titanium alloy Ti-6Al-4V on human bone marrow cell response and on protein adsorption. Biomaterials. 2001;22:1241–51.

Figure captions

Fig.1. Current-time responses during the anodizing process of titanium for the coatings obtained in an electrolyte with (a) HF (b) NaF (c) NH_4F.

Fig.2. XRD spectra of coatings obtained at (a) 10 V (b) 15 V and after heat treatment.

Fig.3. Raman spectra of coatings obtained before (a) and after (b) of heat treatment.

Fig. 4 SEM micrographs of the coatings as anodized at 15 V in an electrolyte containing HF (a-b), NaF (c-d) and NH_4F (e-f).

Fig.5. SEM micrographs of coatings obtained at 15 V in electrolytes containing HF (a-b), NaF (c-d) and NH_4F (e-f), all cases after heat treatment.

Fig.6. SEM micrographs of the coatings as anodized at 10 V in an electrolyte with HF (a-b), NaF (c-d) and NH_4F (e-f).

Fig.7. SEM micrographs of the coatings obtained at 10 V in electrolytes containing HF (a-b), NaF (c-d) and NH_4F (e-f), all cases after heat treatment.

Fig.8. SEM micrographs of osteoblasts cultured on titanium coatings without heat treatment and anodized with an applied voltage of 15 V obtained in an electrolyte with HF (a, b), NaF (c,d), NH_4F (e, f), Titanium unanodized (g, h).

Fig.9. SEM micrographs of osteoblasts cultured on titanium coatings after heat treatment and anodization with an applied voltage of 15 V obtained in an electrolyte with HF (a, b), NaF (c, d), NH_4F (e, f).

Fig.10. Time course (3 to 24h) of adhesion of ASC on titanium anodized with resp. HF, NaF, NH_4F or no coating. Adhered cells (green) were visualized after staining with fluorescent phalloidin (cytoskeleton) and DAPI (blue, nuclei) and fluorescence microscopy. Original magnification 20x.

Table 1

Charge Density for the coatings obtained with different fluoride ion source

Fluoride Ion Source	Charge Density (C/cm^2)	
	15 V	**10 V**
HF	23.61	15.96
NaF	48.44	36.20
NH_4F	87.18	44.58

Table 2

Electrolyte conductivity

Fluoride Ion Source	Conductivity (mS/cm)
HF	16.69
NaF	50.08
NH_4F	70.31

Table 3

The mass fraction of rutile (f_r) for the coatings after heat treatment

Fluoride Ion Source	Mass fraction of rutile	
	15 V	**10 V**
HF	0.73	0.70
NaF	0.79	0.71
NH_4F	0.66	0.85

Table 4

The linear relationship in weight (W_R/W_A) for the coatings after heat treatment

Fluoride Ion Source	Linear Relationship in Weight (W_R/W_A)	
	15 V	**10 V**
HF	5.47	4.10
NaF	5.64	3.84
NH_4F	4.01	4.45

Table 5

Internal diameter and nanotube wall thickness in nm for the coatings obtained with different fluoride ion sources

Fluoride Ion Source	Internal diameter of nanotubes [nm]				Thickness [nm]			
	Without heat treatment		With heat treatment		Without heat treatment		With heat treatment	
	10 V	15 V	10 V	15 V	10 V	15 V	10 V	15 V
	26.22 ± 4.99	66.99 ± 8.96	19.66± 2.97	42.94 ± 10.94	123.87 ± 4.12	229.73 ± 8.79	103.40 ± 17.62	125.18 ± 24.52
NaF	31.70 ± 6.39	66.84 ± 11.70	20.84± 6.22	35.36 ± 5.23	179.59 ± 11.01	293.85 ± 9.59	164.38 ± 41.70	266.96 ± 44.39
$_4$F	27.01 ± 4.48	48.88 ± 5.19	19.50± 4.60	42.93 ± 9.93	236.45 ± 11.89	400.80 ± 17.28	196.93 ± 35.08	301.36 ± 38.28

Table 6

Contact angle measurements for samples anodized in different electrolytes.

Fluoride Ion Source	Without Heat treatment		With Heat treatment	
	10 V	**15 V**	**10 V**	**15 V**
HF	113.67 ± 4.58	42.21 ±1.35	20.67 ± 1.75	6.80 ± 0.18
NaF	107.31 ± 13.20	31.48 ±2.55	19.35 ± 0.13	13.17 ±0.81
NH_4F	52.50 ± 1.55	31.40 ± 2.36	17.79 ± 0.20	21.27 ± 0.83
c.p Ti	51.71 ± 0.71			

Table 7

Surface free energy calculations $mJ.m^{-2}$ for samples anodized in different electrolytes.

Fluoride Ion Source	Without Heat treatment		With Heat treatment	
	10 V	**15 V**	**10 V**	**15 V**
HF	15.00 ± 2.60	58.17 ±0.74	68.50 ± 0.68	72.30 ± 0.02
NaF	18.60 ± 8.01	63.77 ±1.21	69.00 ± 0.05	70.96 ±0.21
NH_4F	52.3 ± 0.91	63.8 ± 1.13	68.94 ± 1.81	68.27 ± 0.32
c.p Ti	52.77 ± 0.41			

Table 8

Cytotoxicity of the samples by using MTT assay

Sample	Mitochondrial activity (%)
HF	97.72 ± 0.021
NaF	96.39 ± 0.016
NH_4F	100 ± 0.009
c.p Ti	100 ± 0.017

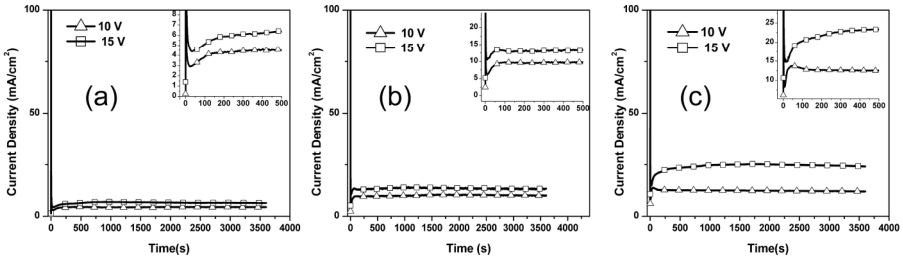

Fig.1. Current-time responses during the anodizing process of titanium for the coatings obtained in an electrolyte with (a) HF (b) NaF (c) NH4F.

96x33mm (600 x 600 DPI)

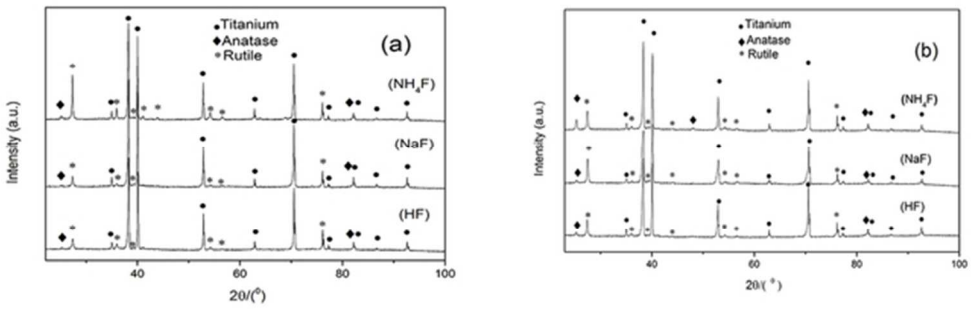

Fig.2. XRD spectra of coatings obtained at (a) 10 V (b) 15 V and after heat treatment.

55x18mm (300 x 300 DPI)

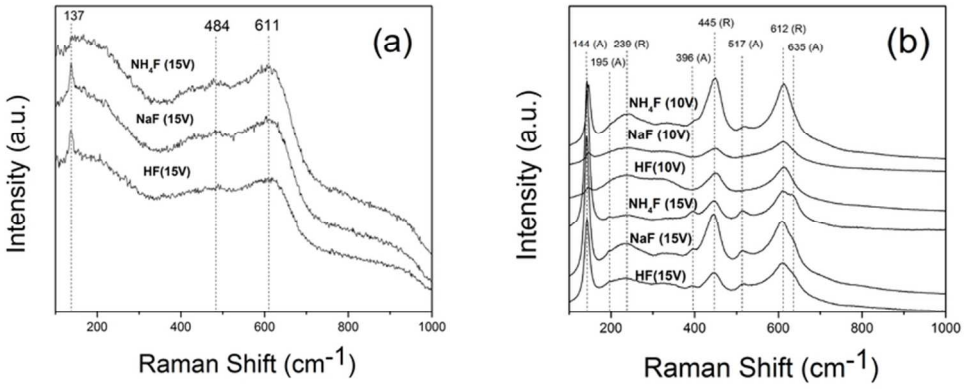

Fig.3. Raman spectra of coatings obtained before (a) and after (b) of heat treatment.

75x33mm (300 x 300 DPI)

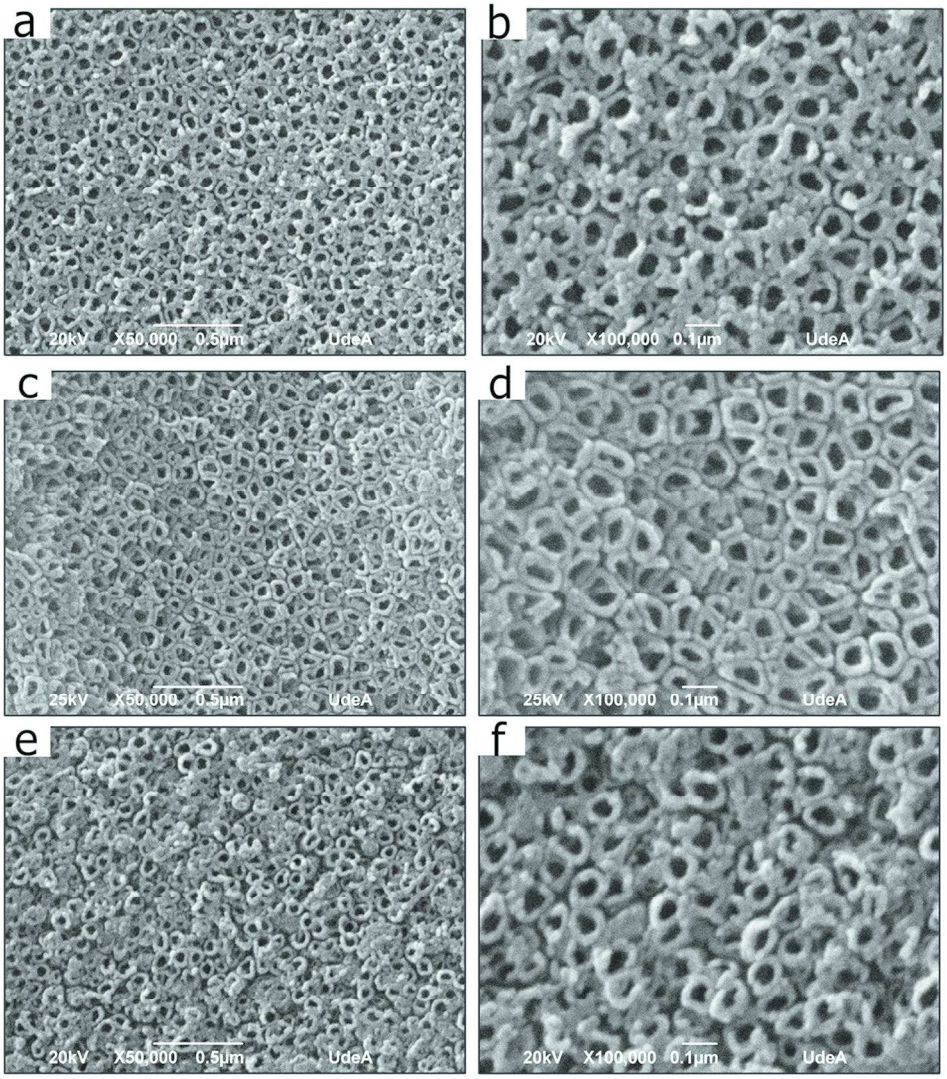

Fig. 4 SEM micrographs of the coatings as anodized at 15 V in an electrolyte containing HF (a-b), NaF (c-d) and NH4F (e-f).

190x212mm (300 x 300 DPI)

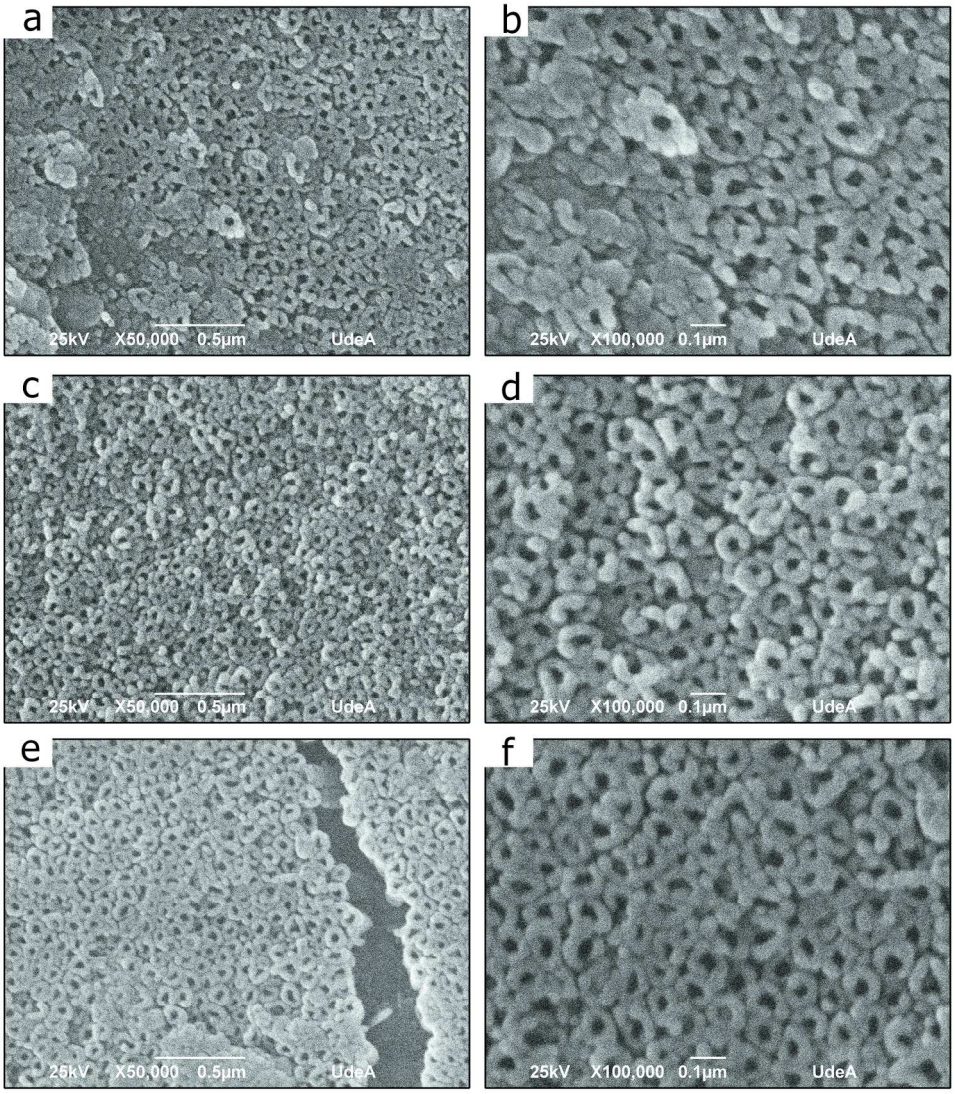

Fig.5. SEM micrographs of coatings obtained at 15 V in electrolytes containing HF (a-b), NaF (c-d) and NH4F (e-f), all cases after heat treatment.

191x215mm (300 x 300 DPI)

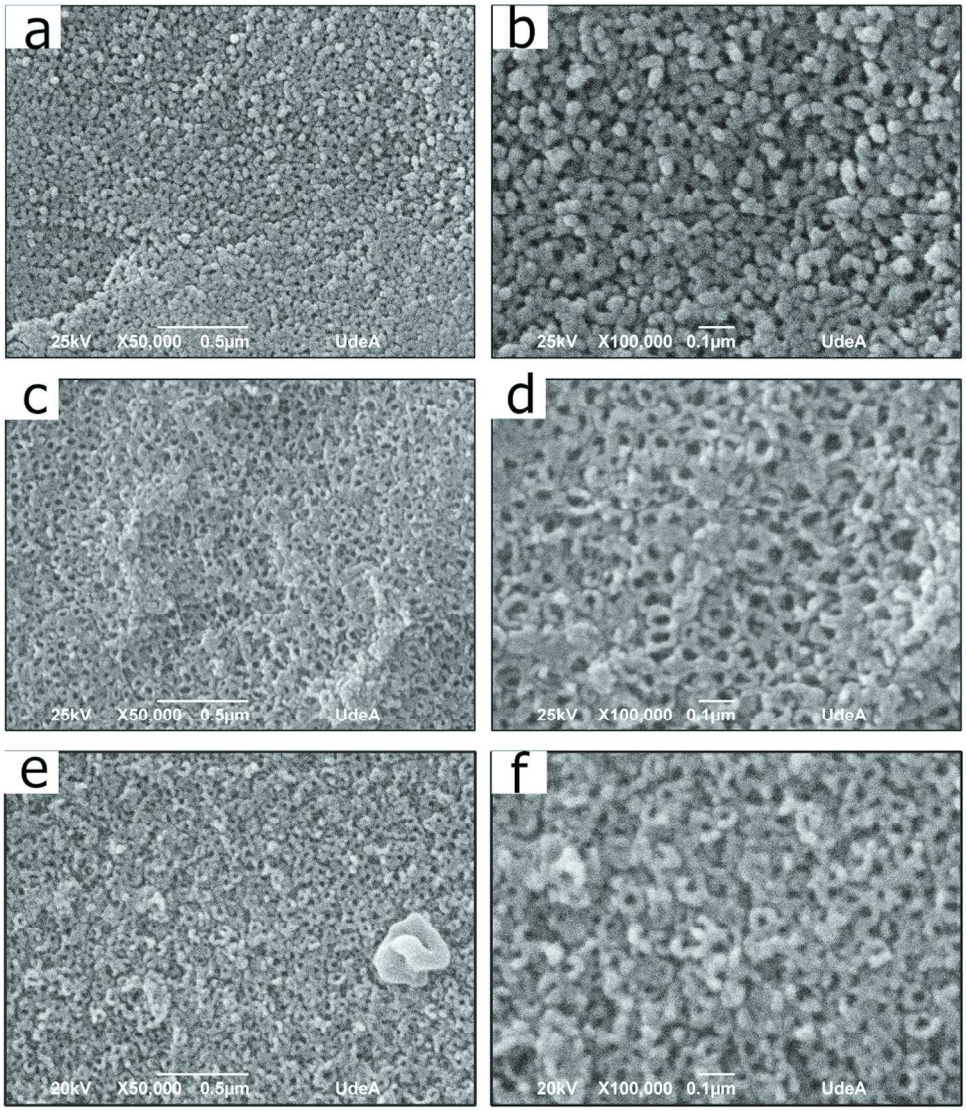

Fig.6. SEM micrographs of the coatings as anodized at 10 V in an electrolyte with HF (a-b), NaF (c-d) and NH4F (e-f).

195x224mm (300 x 300 DPI)

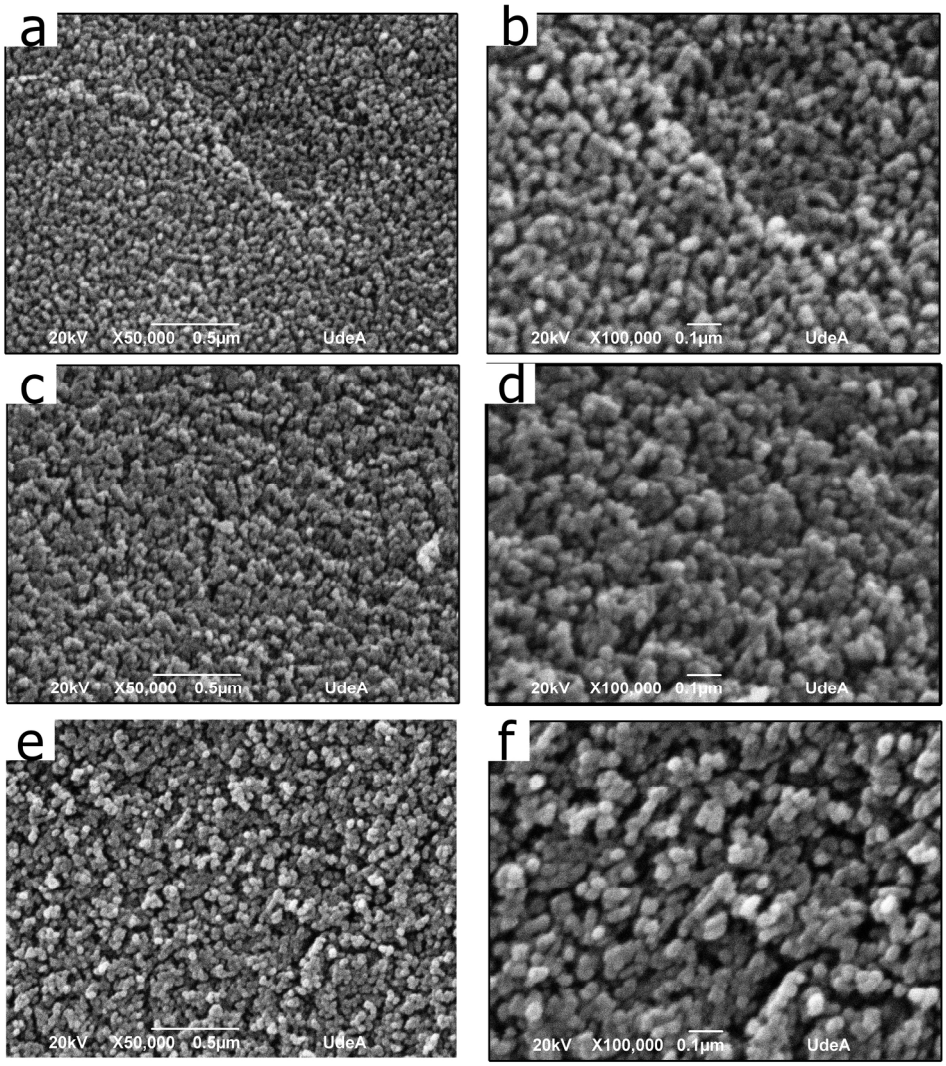

Fig.7. SEM micrographs of the coatings obtained at 10 V in electrolytes containing HF (a-b), NaF (c-d) and NH4F (e-f), all cases after heat treatment.

188x209mm (300 x 300 DPI)

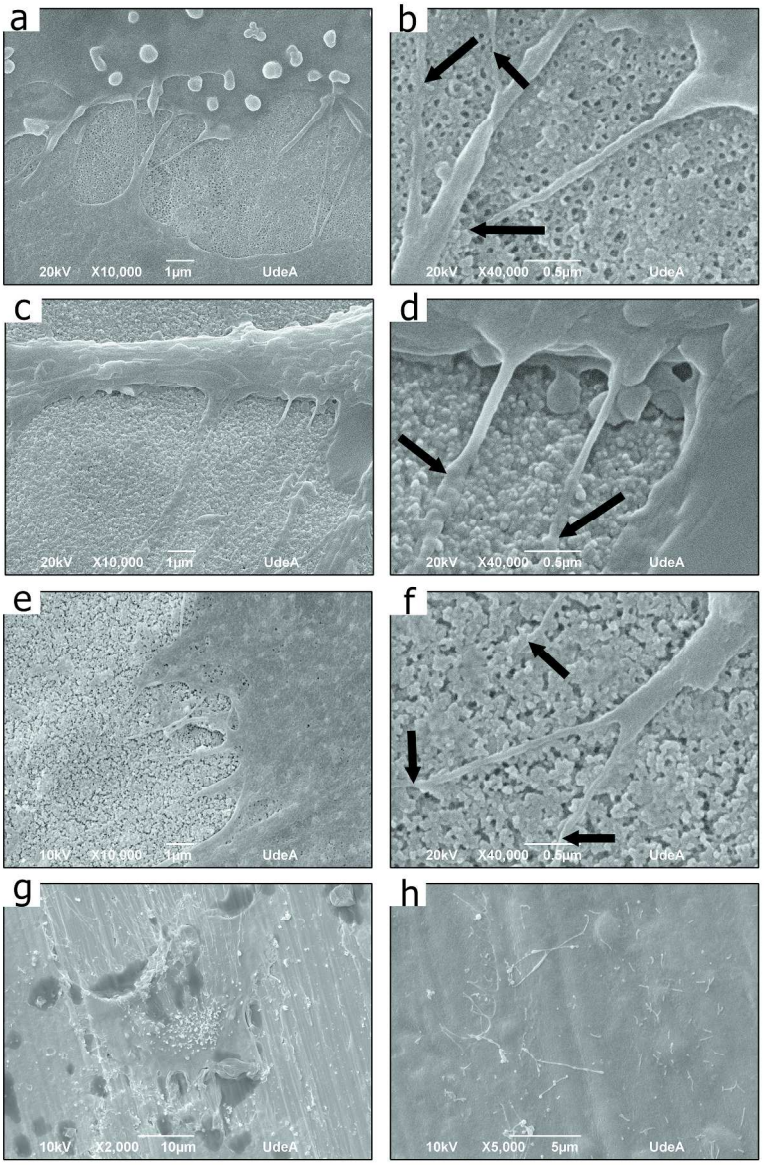

Fig.8. SEM micrographs of osteoblasts cultured on titanium coatings without heat treatment and anodized with an applied voltage of 15 V obtained in an electrolyte with HF (a, b), NaF (c,d), NH4F (e, f), Titanium unanodized (g, h).

229x350mm (300 x 300 DPI)

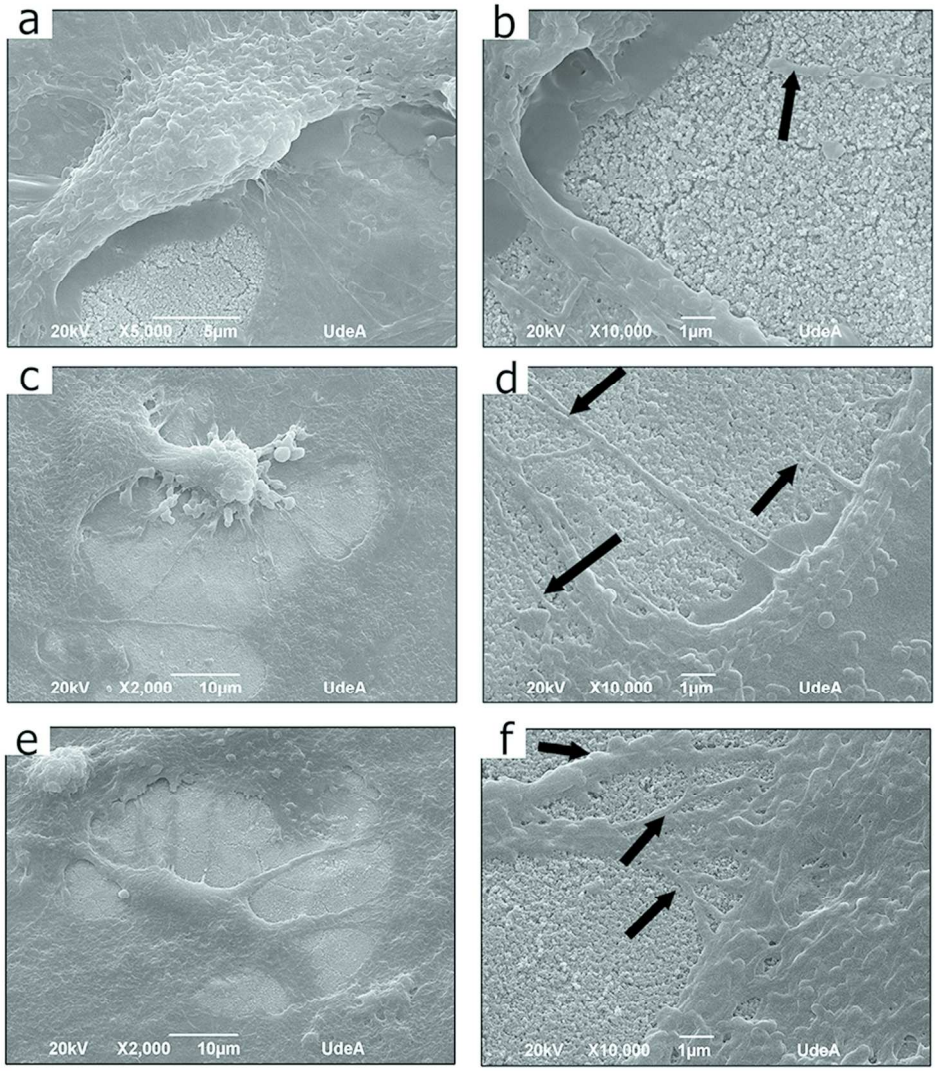

Fig.9. SEM micrographs of osteoblasts cultured on titanium coatings after heat treatment and anodization with an applied voltage of 15 V obtained in an electrolyte with HF (a, b), NaF (c, d), NH4F (e, f).

191x216mm (300 x 300 DPI)

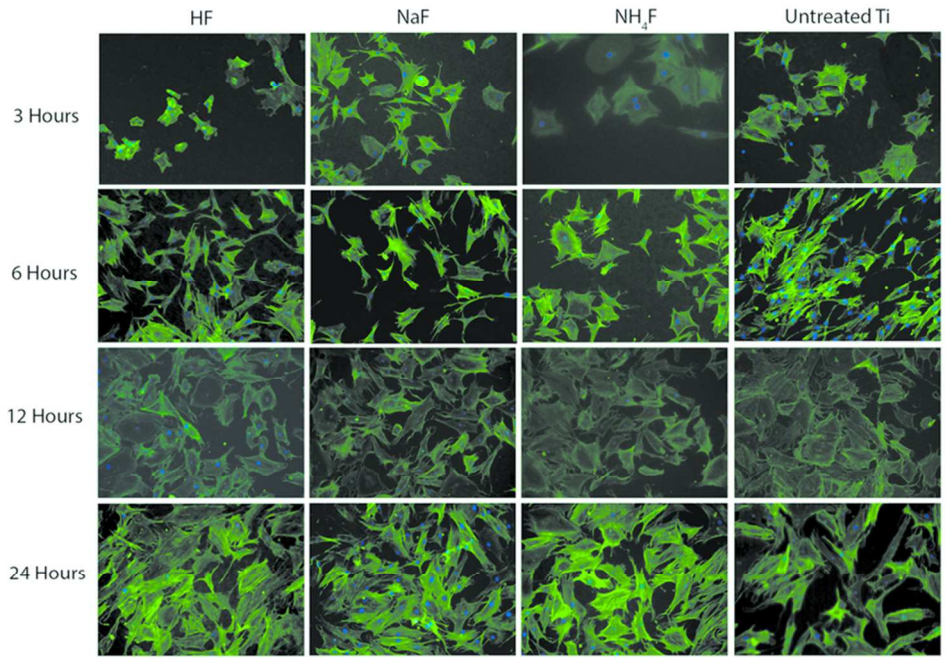

Fig.10. Time course (3 to 24h) of adhesion of ASC on titanium anodized with resp. HF, NaF, NH4F or no coating. Adhered cells (green) were visualized after staining with fluorescent phalloidin (cytoskeleton) and DAPI (blue, nuclei) and fluorescence microscopy. Original magnification 20x.

78x53mm (300 x 300 DPI)